ACS MATERIALS LETTERS

Cite This: ACS Materials Lett. 2019, 1, 354−361

www.acsmaterialslett.org

LETTER

Flexible Solid-State Electrolyte with Aligned Nanostructures Derived from Wood

Jiaqi Dai,[†,▽] Kun Fu,[†,‡,▽] Yunhui Gong,[†,‡,▽] Jianwei Song,[†] Chaoji Chen,[†] Yonggang Yao,[†] Glenn Pastel,[†] Lei Zhang,[‡] Eric Wachsman,[*,†,‡] and Liangbing Hu[*,†,‡]

[†]Department of Materials Science and Engineering, University of Maryland, College Park, Maryland 20742, United States

[‡]Maryland Energy Innovation Institute, University of Maryland, College Park, Maryland 20742, United States

Supporting Information

ABSTRACT: **Solid-state Li-batteries (SSLiBs) with solid-state electrolytes (SSEs) can potentially block Li dendrite penetration, enabling the application of metallic lithium anodes to achieve high energy density with improved safety. The ion transport behavior and ionic conductivity in Li-ion batteries is significantly influenced by the tortuosity of the electrode and electrolyte materials. Low-tortuosity structures with straight ion pathways are highly desirable yet very difficult to achieve in solid-state ion conductors. Templating from wood, for the first time, we developed a highly conductive garnet framework with multiscale aligned mesostructure through a scalable, top-down approach. Ion-conductive poly(ethylene oxide) (PEO) was incorporated into the mesoporous, wood-templated aligned garnet nanostructure, resulting in a flexible solid-state composite electrolyte. The synergistic integration of the aligned garnet with soft, mechanically robust polymer results in both a high ionic conductivity (1.8×10^{-4} S/cm at room temperature) and good mechanical flexibility. This work provides a new direction for developing low-tortuosity, fast ion conductors inspired by nature.**

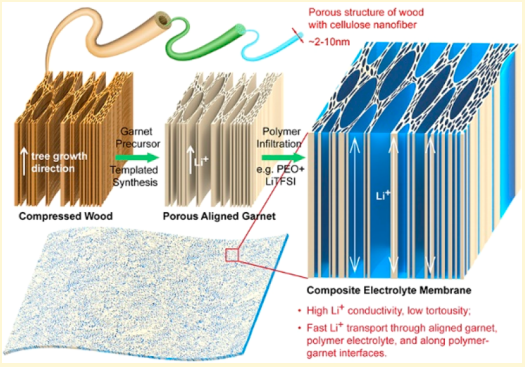

Toward the development of high-energy-density batteries, the metallic lithium (Li) anode is one of the most promising alternatives to replace conventional anode materials, because of its highest gravimetric energy density (3860 mAh/g) and lowest electrochemical potential (~3.04 V against the standard hydrogen electrode).[1−3] However, its application in conventional cell configurations is greatly hindered by safety concerns, including liquid electrolyte decomposition and the high combustibility of organic electrolyte, as well as solid-electrolyte-interface (SEI) formation.[4−8] In particular, Li dendrite growth and propagation can penetrate through the polymer separator in conventional full cell configurations and cause catastrophic short circuits. Therefore, extensive studies have focused on SSEs with great ionic conductivity and good mechanical strength that can address Li dendrite-dominated challenges.[9,10]

In the past several decades, many outstanding solid electrolyte materials, including conductive oxides,[11−16] phosphates, hydrides, halides, sulfides,[17−19] and polymer-based composites[20−23] have been developed for solid-state batteries.[24] Among various inorganic solid electrolytes, garnet-type $Li_7La_3Zr_2O_{12}$ (LLZO) is one of the most important and appealing candidates for its high ionic conductivity (10^{-4}−10^{-3} S/cm) at room temperature (RT),[13] wide voltage window (0.0−6.0 V),[25,26] and exceptional chemical stability against Li metal.[27,28] Among various organic solid electrolytes, plasticized poly(ethylene oxide) (PEO) enhanced with inorganic oxide fillers is widely used, because of its ionically conductive properties in an amorphous state, scalability, electrochemical stability against lithium metal, and reasonable mechanical strength.[29,30] Moreover, recent developments suggest that inorganic-ion-conductor−polymer composite electrolytes (CPEs) with engineered nanostructures can give rise to further improvements in ionic conductivity,[31−33] electrochemical stability,[34] and mechanical strength.[35] For example, a solid state CPE proposed by Cui et al., consisting of polyacrylonitrile (PAN)-$LiClO_4$ with $Li_{0.33}La_{0.557}TiO_3$ (LTO) nanowires, exhibited outstanding ionic conductivity at room temperature and good electrochemical stability.[36] Several other solid-state CPEs enhanced with three-dimensional (3D) flexible garnet-type LLZO networks were also reported to exhibit high ionic conductivity at room temperature and good mechanical strength.[37,38] However, the inorganic components in these CPEs are either isolated particles or random fibrils with a high tortuosity that would increase the transport distance of ions. As

Received: May 27, 2019
Accepted: August 9, 2019
Published: August 9, 2019

DOI: 10.1021/acsmaterialslett.9b00189
ACS Materials Lett. 2019, 1, 354−361

defined by $\sigma_{eff} = \sigma_0\epsilon/\tau$ and the Bruggeman relationship $\sigma_{eff} = \sigma_0\epsilon^{\alpha}$, where σ_0 and σ_{eff} are the intrinsic and the effective conductivity of the conducting phase, respectively, ϵ is the volume fraction of the conductive phase, and α is the Bruggeman exponent; the ion transport behavior and, therefore, the ionic conductivity can be significantly influenced by the tortuosity (τ) of the electrode and electrolyte materials, especially when the electrodes and/or electrolytes are thick.[39] Recent developments on ultrathick electrodes demonstrated that the ionic conductivity and electrochemical performances of the cell was greatly enhanced, because of the faster ion transport imparted by straight pores with low tortuosity.[40,41] In this context, constructing SSE nanostructures with low tortuosity is highly desirable to achieve a high ionic conductivity. Recent works have shown that aligned structures prepared by ice-templating method[42,43] and track-etching technique[44] can effectively guide ion transport and enhance the ionic conductivity of solid electrolytes.[45]

Inspired by the aligned structure of natural wood, we report a highly ionically conductive garnet network with well-aligned mesostructures through templated synthesis. Wood was adopted as a sacrificial template resulting in multiscale aligned porosity, low tortuosity, and high specific surface area of garnet mesostructures. Because of the high ionic conductivity, good chemical stability with Li anodes, and wide electrochemical window, in this work, we chose garnet-type LLZO as the model system to fabricate a low tortuosity and aligned solid-state electrolyte. A composite electrolyte was developed by incorporating PEO polymer electrolyte into the aligned garnet templated by wood, which is called garnet-wood (Figure 1). The

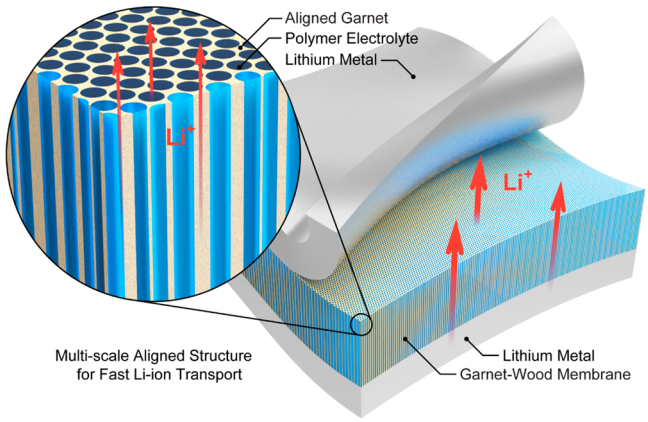

Figure 1. Schematic of multiscale aligned mesoporous garnet $Li_{6.4}La_3Zr_2Al_{0.2}O_{12}$ (LLZO) membrane incorporated with polymer electrolyte in a lithium symmetric cell. The garnet-wood possesses multiscale aligned mesostructure derived from natural wood, which enables the unobstructed Li ion transport along the garnet/polymer interface, through garnet, and through polymer electrolyte.

polymer electrolyte provides additional transport pathways and reinforces the mechanical strength of the composite structure. Li ions can effectively transport through garnet, polymer, and along garnet/polymer interfaces. As a result, the garnet-wood membrane delivers an outstanding ionic conductivity of 1.8×10^{-4} S/cm at room temperature. Based on this concept, the design principle and fabrication process for aligned garnet-wood electrolyte can be extended to other types of solid-state electrolytes.

Basswood was chosen as a template to develop the aligned garnet solid-state electrolyte framework, because of its high growth rate, low cost, and high porosity. The wood template was obtained after partially removing lignin from a piece of natural basswood by chemical treatment, followed by compressing and slicing perpendicular to the longitudinal direction (natural growth direction) of the wood (Figure 2a). Mechanical pressing was used to densify the wood. Additional hydrogen bonds formed between adjacent cellulose fibers during densification, which maintains the dense structure of the framework (Figures S1 and S2 in the Supporting Information). The morphological changes induced by mechanical compression were investigated with scanning electron microscopy (SEM) measurements of multiple specimens. Before compressing, microchannels in the wood have proximal cylindrical shape with diameters between 10−50 μm, on average (Figures 2b and 2d). After compression, most of the previously observed microchannels were squeezed into crack-shaped gaps, and some of the adjacent channels became connected (Figures 2c and 2e). The densification method gives a similar structure, regardless of the wood species (see Figures S3 and S4 in the Supporting Information). Although these open channels in wood were severely deformed after compression, their highly aligned multiscale porous structure remained unchanged (Figure 2f) and showed great absorbency when immersed into the precursor solution. For instance, after soaking for 48 h and drying in vacuum at 70 °C for 4 h, the mass of the wood template increased 27.8%, from 2.7 mg to 3.45 mg (see Figure S5 in the Supporting Information). The high absorbency of wood template can be attributed to both the hydrophilic nature of wood cellulose and the capillary forces in the aligned multiscale pores. The high absorption of precursor solution, pliable nature of the template pores, and scalability of the procedure are indicative of a cost-effective and productive method for fabricating SSEs with aligned mesostructures.

The wood with infiltrated garnet precursor was calcined at 800 °C for 4 h in oxygen to obtain the LLZO membrane (see Figure S6 in the Supporting Information). The wood template with aligned channels has two unique functions. First, the free channels in the wood template provide reservoirs to supply precursor solutions to the template combustion reaction. Second, the aligned nanofibers with a diameter of 2−10 nm in the wood template serve as sacrificial pore formers for additional aligned porosity in the garnet membrane. Morphological changes after calcination were characterized by SEM. The aligned porous structure from the wood template was inherited in the resulting garnet framework at both the microscale (Figure 3a) and nanoscale (Figure 3b). The thickness of the garnet membrane was controlled by the thickness of the wood template. SEM image shows that the low-tortuosity channels are highly aligned and penetrate throughout the entire garnet membrane (see Figures S7 and S8 in the Supporting Information). The well-aligned garnet membrane developed directly from a wood template is flexible after infiltration with the PEO-based polymer electrolyte (Figure 3c). X-ray diffraction (XRD) was employed to identify the crystal phase of the garnet membrane. The XRD pattern of the aligned mesoporous garnet synthesized using wood template (Figure 3d) matched well with the cubic-phase garnet $Li_5La_3Nb_2O_{12}$ (JCPDS File No. 80-0457), despite minor peak shifts at higher angles due to aluminum (Al) doping and variations in Li concentration. As a representative structure of fast lithium-ion-conductive garnet, $Li_5La_3M_2O_5$ (M = Nb, Ta) is widely used as a reference to distinguish conductive garnet phases from non-

DOI: 10.1021/acsmaterialslett.9b00189
ACS Materials Lett. 2019, 1, 354−361

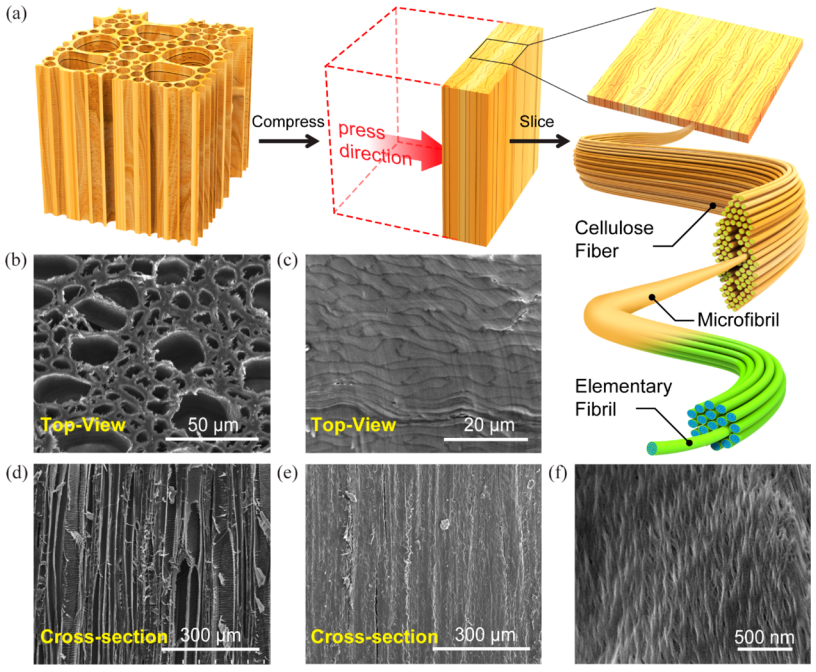

Figure 2. Characterization of the wood template: (a) illustrations of the wood template fabrication through compressing and slicing; (b) SEM image (top view) of pristine wood; (c) SEM image (top view) of compressed wood, with the apparent diameter reduction of the wood microchannels after compression; (d, e) cross-sectional SEM images comparing pristine wood (panel (d)) and compressed wood (panel (e)), in which the channels are closed but the highly aligned structure is preserved; (f) SEM image of the aligned nanofiber with a diameter of ~10 nm.

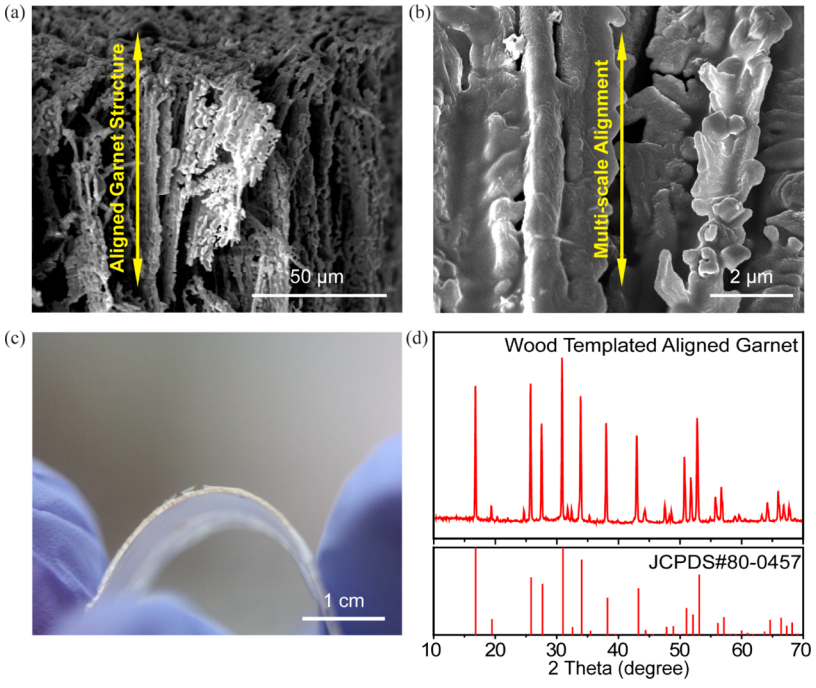

Figure 3. Calcination of the aligned garnet templated by wood: (a, b) cross-sectional SEM images showing the alignment of channels at both the microscale level (panel (a)) and the nanoscale level (panel (b)); (c) photograph of the flexible garnet-wood consisting of the aligned mesoporous garnet and PEO-based polymer electrolyte; (d) XRD pattern of the aligned garnet matches JCPDS File No. 90-0457, which verifies the cubic garnet structure.

conductive ones.[46] The good XRD pattern match of the aligned mesoporous garnet with JCPDS File No. 80-0457 verifies that the wood-templated garnet is the conductive cubic phase.

High-resolution transmission electron microscopy (HRTEM) of the resulting aligned garnet reveals the clear, well-crystallized lattice structure of the garnet (Figure 4a). The Miller indices were calculated from the corresponding fast Fourier transform (FFT) pattern (inset of Figure 4a) and the lattice constant derived from the HRTEM and FFT is 12.982 Å, which agrees with previously reported values.[47] Crystal grains with various orientations can be clearly distinguished in the HRTEM image of a larger garnet particle broken off from the

DOI: 10.1021/acsmaterialslett.9b00189
ACS Materials Lett. 2019, 1, 354−361

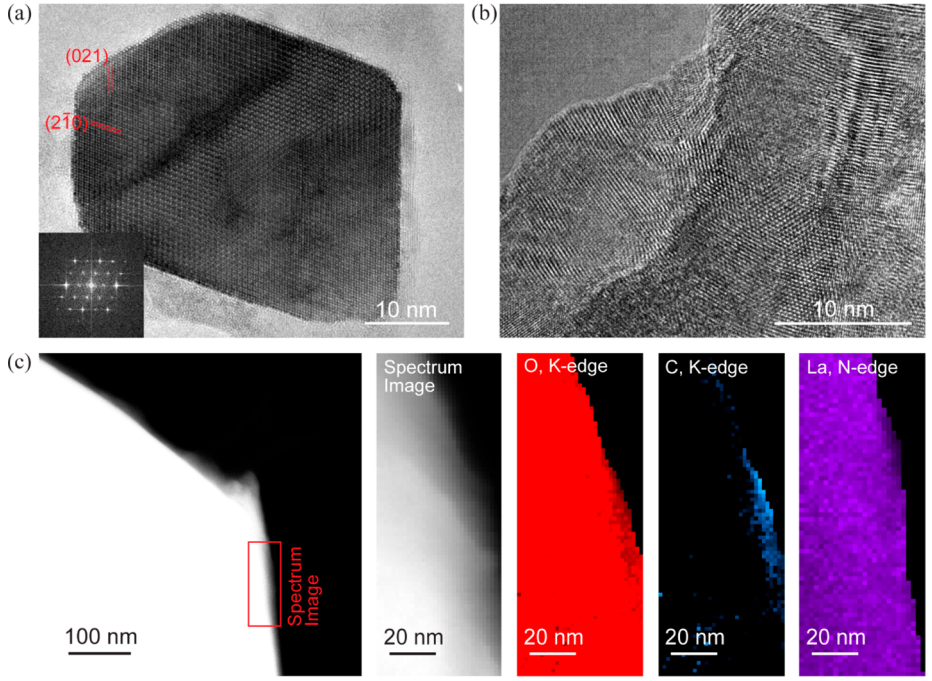

Figure 4. TEM characterization of garnet crystal structure: (a) HRTEM image of a nanoparticle broken off from the aligned garnet showing the (2$\bar{1}$0) and (021) lattice planes (inset graph shows the FFT patterns of the HRTEM image); (b) TEM image of the edge of a garnet nanoparticle, showing a clear multicrystalline structure; and (c) EELS spectrum of the garnet surface showing the ROI, spectrum image, and relative composition map of O, C, and La, respectively.

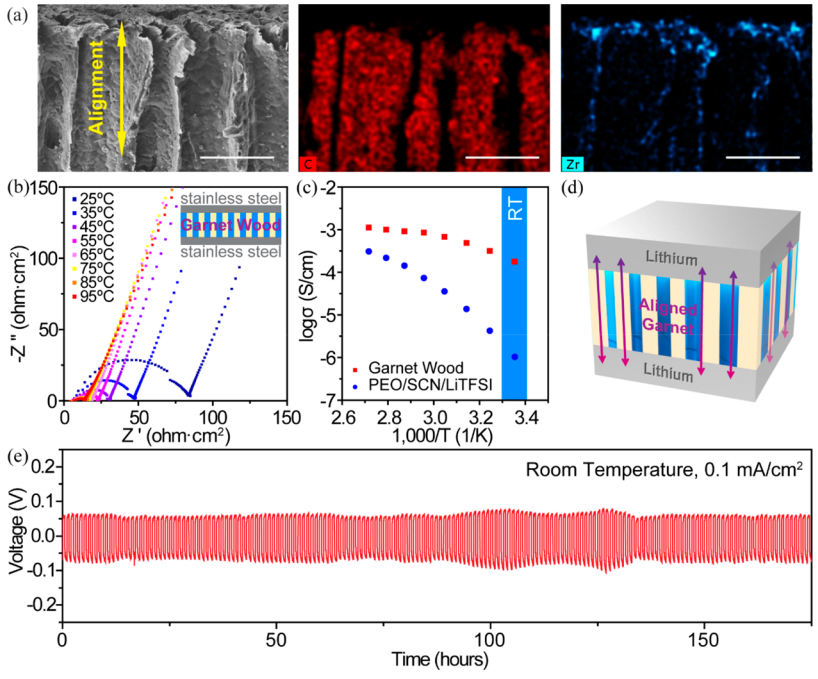

Figure 5. Electrochemical characterizations of the garnet-wood with aligned mesoporous structure. (a) SEM and its corresponding EDX images showing the complete, uniform infiltration of polymer electrolyte throughout the aligned garnet. Scale bars = 100 μm; (b) Nyquist plot showing the decrease in the impedance of the garnet-wood membrane with increasing temperature (the inset schematic shows the structure of the testing cell); (c) comparison of the ionic conductivity of the garnet-wood and PEO-based polymer electrolyte at different temperatures, the blue region indicates measurements performed within the range of room temperature (RT); (d) schematic of the lithium symmetric cell with garnet-wood, showing the low tortuosity, fast lithium transport pathways; and (e) galvanostatic cycling of Li/garnet-wood/Li with a current density of 0.1 mA/cm^2 at RT.

structure (Figure 4b). The TEM results indicate that the aligned mesoporous garnet has a highly crystallized, well-connected multicrystalline structure. Electron energy loss spectroscopy (EELS) was employed to analyze the composition of the garnet membrane. Figure 4c shows the EELS spectrum with the region of interest (ROI) outlined. EELS mapping indicates the relative

DOI: 10.1021/acsmaterialslett.9b00189
ACS Materials Lett. 2019, 1, 354−361

composition and distribution of oxygen, carbon, and lanthanum. The overlapping region of O k-edge signal and La n-edge signal identifies the location of LLZO. Although the C k-edge signal is rare throughout the sample, a small overlapping region of the O k-edge signal and C k-edge signal was identified, which indicates that the Li_2CO_3 impurities caused by calcining in oxygen is minimal.

The garnet-wood SSE was fabricated by infiltrating PEO polymer electrolyte into the aligned garnet. Figure 5a characterizes the polymer infiltration with energy-dispersive X-ray spectroscopy (EDX). The evenly distributed carbon signal from the top, down to the aligned garnet channels indicates complete and uniform infiltration of the polymer electrolyte, which is crucial for establishing sufficient Li ion transport pathways (see Figure S9 in the Supporting Information). As suggested in the literature, there are three possible Li-ion transport pathways. The first pathway is the aligned PEO polymer electrolyte, whose bulk ionic conductivity (without fillers) is usually as low as 10^{-6} S/cm at room temperature (see Figure S10 in the Supporting Information).[48] The second pathway is the aligned garnet/polymer interface. At the interface, the aligned mesoporous garnet behaves like a ceramic filler that can induce changes to the polymer segmental dynamics and, therefore, influences Li-ion transport. Intensive studies on the influence of fillers on the ionic conductivity of polymer electrolyte suggest that the existence of ceramic fillers reduces the crystallinity of polymer matrix. Positively charged oxygen vacancies in ceramic fillers acting as Lewis acid sites can promote Li-ion transport by anion coupling and provide preferential conductive pathways.[49−51] The third pathway is transport through the high volume percentage (~68%) aligned garnet nanostructure. Recent studies indicate that, among the three transport pathways in garnet−polymer composite electrolyte systems, conduction through the garnet phase is the most preferred, evidenced by tracking isotope-labeled Li-ion migration using nuclear magnetic resonance (NMR).[52] Note that the typical bulk ionic conductivity of dense LLZO achieved in our laboratory using the same composition is up to 2.2×10^{-4} S/cm at room temperature. However, this bulk ionic conductivity is difficult to achieve in conventional mesoporous structures, because of the highly tortuous transport pathways caused by random pores and insufficient solid−solid interfacial contact at the numerous pore gaps.[45,53] In contrast, the low tortuosity of the aligned mesoporous garnet structure enables unobstructed Li ion transport along the normal direction of the flexible garnet-wood, which effectively promotes ionic conductivity.

The ionic conductivity of the garnet-wood was characterized by electrochemical impedance spectroscopy (EIS). A garnet-wood membrane (area of 0.178 cm^2, 150 μm thick) was assembled into symmetric cells with stainless steel as the blocking electrodes and scanned from 1 MHz to 100 mHz. Figure 5b shows the Nyquist plot of the electrolyte membrane tested from 25 °C to 95 °C. The experimental ionic conductivity is calculated using the electrolyte membrane thickness and area, and the results are shown in Figure 5c. The garnet-wood membrane achieved an ionic conductivity of 1.8×10^{-4} S/cm at room temperature. As the operating temperature is increased, the intersection of the semicircle with the real impedance axis decreased, indicating an improved ionic conductivity with elevated temperature (Figure 5b). At 95 °C, the ionic conductivity increased to 1.1×10^{-3} S/cm, which represents a factor of 6.3 improvement above the room-temperature performance. The temperature dependence of the ionic conductivity for the garnet-wood can be expressed by the Arrhenius equation:

$$\sigma = A \exp\left(-\frac{E_A}{kT}\right)$$

where σ is the total ionic conductivity of garnet-wood, A the pre-exponential factor, T the absolute temperature, E_A the activation energy of garnet-wood, and k the Boltzmann constant.[54] The calculated activation energy of garnet-wood is 0.38 eV, which can be decreased further by adjusting the proportion of polymer electrolyte. This effect is due to various enhancement effects, including the increase in the volume fraction of amorphous conducting phase as well as the improvement in the long-range polymer chain mobility.[49]

As a proof-of-concept, a Li metal/garnet-wood/Li metal symmetrical cell was fabricated, and a Li stripping/plating test was performed at room temperature (Figure 5d). Figure 5e shows a characteristic 180 h of the cycling at a current density of 0.1 mA/cm^2 for 30 min in each direction. The voltage response of the symmetric cell stabled at 50 mV with slight fluctuations. The symmetrical cell cycled well for over 600 h with small polarization (see Figure S11 in the Supporting Information). Cyclic voltammetry (CV) curve of the symmetrical cell suggests that the electrolyte is stable up to 6 V (see Figure S12 in the Supporting Information). Garnet-wood was sandwiched with lithium metal as counter and reference electrodes and stainless steel was used as a working electrode. The long-term cycling performance indicates that the garnet-wood membrane enhanced with aligned mesoporous garnet can enable fast and stable ion transport. The wide voltage window suggests that the electrolyte meets the voltage stability requirements of high-voltage oxide cathodes. In addition, the polymer electrolyte also largely improves the mechanical flexibility of the aligned garnet, enabling its use in Li metal batteries.

In summary, garnet-wood composite SSE with a multiscale aligned mesoporous structure is reported for the first time. The scalable compressed wood template results in the unique low tortuosity and high surface area mesostructure that is critical to the improved electrochemical performance and mechanical stability. Ionically conductive polymer serves as a matrix to reinforce the mechanical strength of the aligned mesoporous garnet membrane and provide additional ion transport pathways through the amorphous conductive phase and the garnet-polymer interfaces. Benefiting from these structural merits in combination with the intrinsic high ion conductivity and low tortuosity of the aligned mesoporous garnet, the garnet-wood composite electrolyte achieves a high Li ion conductivity of 1.8×10^{-4} S/cm at room temperature and 1.1×10^{-3} S/cm at 95 °C. This is close to the bulk conductivity of garnet itself and moreover exhibits an enhanced contribution from the garnet/polymer interface. The garnet-wood demonstrates great potential as a low-tortuosity structure for highly conductive SSE and it also provides a model study for the design and optimization of solid-state CPEs.

EXPERIMENTAL SECTION

Materials Preparation. The wood template was prepared by slicing the compressed wood perpendicular to the longitudinal direction (natural growth direction). To prepare the compressed wood, basswood blocks were boiled in a water solution of mixed NaOH (≥97.0%, Aldrich) and Na_2SO_3 (≥98.0%, Aldrich) with a mole ratio of 5:1 for 7 h, followed

DOI: 10.1021/acsmaterialslett.9b00189
ACS Materials Lett. 2019, 1, 354−361

by immersion in boiling deionized water to remove any remaining chemicals. The basswood blocks were then compressed at 100 °C with a pressure of 5 MPa.

The garnet precursor solution was prepared by dissolving stoichiometric $LiNO_3$ (≥99.0%, Aldrich), $La(NO_3)_3$ (≥99.9%, Aldrich), $Al(NO_3)_3{\cdot}9H_2O$ (≥98.0%, Aldrich), $ZrO(NO_3)_2{\cdot}xH_2O$ (99.9%, Aldrich), and acetic acid (≥99.7%, Aldrich) in ethanol (≥99.8%, Aldrich) at room temperature under magnetic stirring. The total cation concentration of the precursor solution was 2 mol/L. 15% excess lithium nitrate was added to compensate for the loss of lithium at high calcination temperatures.

The wood template was soaked in the above-mentioned solution for 48 h to impregnate the garnet precursors. Excess solution was wiped off from the surface and the sample was dried at 70°C for 4 h. Subsequently, two 5-h thermal treatments were conducted in oxygen—first at 400 °C and then at 800 °C—to burn off the organics and sinter the dispersed precursors. The heating process was carefully controlled with a ramp rate of 10 °C/min to retain the microstructure of the wood template. Garnet nanoparticles and nanofibers for TEM studies were obtained by grinding and sonicating the garnet membrane in isopropanol (IPA).

The PEO-based polymer electrolyte was prepared by dissolving PEO (Mv = 600 000, Aldrich) with bis-(trifluoromethane)sulfonimide lithium salt (LiTFSI, ≥99.85%, Aldrich, EO:Li^+ = 8:1) into acetonitrile (anhydrous, 99.8%, Aldrich) under magnetic stirring in an argon-filled glovebox at room temperature. 15 wt % succinonitrile (SCN, 99%, Aldrich) was added into the solution and the mixture was magnetically stirred until SCN completely dissolved. The drop-cast polymer electrolyte in the aligned mesoporous garnet (garnet-wood) was fully dried in vacuum at room temperature for 1 h before electrochemical testing.

Materials Characterizations. XRD was performed on a Bruker D8 Avance system using Cu K radiation. SEM images and their corresponding EDX images were obtained using a Hitachi SU-70 field-emission SEM system that was equipped for energy-dispersive X-ray spectrometry (EDX). TEM images were obtained using a JEM 2100 field-emission gun TEM system that was equipped for electron energy-loss spectrometry (EELS) studies. FFT image was computed from the high-resolution TEM image, using the Gatan Microscopy Suite. The EIS measurement was performed with a Solartron-1260 impedance gain phase analyzer on symmetric cells consisting of the garnet-wood between stainless steel plates as blocking electrodes. The cells were rested in an environmental chamber for 30 min at the predetermined temperature before each EIS test to reach thermal equilibrium and then scanned from 1 MHz to 100 mHz to acquire the impedance curves at various temperatures. The Li stripping/plating tests were performed with a BioLogic VMP_3 multichannel potentiostat on symmetric cells consisting of the garnet-wood between Li metal foils as electrodes. The cells were cycled at a current density of 0.1 mA/cm^2 for 30 min in each direction at room temperature in an argon-filled glovebox.

■ ASSOCIATED CONTENT

Supporting Information

The Supporting Information is available free of charge on the ACS Publications website at DOI: 10.1021/acsmaterialslett.9b00189.

Photographs and SEM images of pristine wood and compressed wood of various species, weight change of the wood template during infiltration, photographs and SEM images of garnet-wood, ionic conductivity of polymer electrolyte at various temperatures, additional galvanostatic cycling data of garnet-wood symmetric cells, and cyclic voltammetry (CV) curve of garnet-wood (PDF)

■ AUTHOR INFORMATION

Corresponding Authors

*E-mail: ewach@umd.edu (E. Wachsman).
*E-mail: binghu@umd.edu (L. Hu).

ORCID

Chaoji Chen: 0000-0001-9553-554X
Eric Wachsman: 0000-0002-0667-1927
Liangbing Hu: 0000-0002-9456-9315

Author Contributions

[∇]These authors contributed equally.

Notes

The authors declare no competing financial interest.

■ ACKNOWLEDGMENTS

The work was supported by the U.S. Department of Energy EERE (Contract No. DE-EE0007807). We would like to acknowledge Dr. Yongfeng Li, Dr. Tian Li, and Patric Ayerle (University of Maryland) for their valuable suggestions on wood processing. The Maryland NanoCenter (AIMLab) is also graciously acknowledged.

■ REFERENCES

(1) Kang, B.; Ceder, G. Battery Materials for Ultrafast Charging and Discharging. *Nature* **2009**, *458*, 190−193.
(2) Armand, M.; Tarascon, J.-M. Building Better Batteries. *Nature* **2008**, *451*, 652−657.
(3) Choi, J. W.; Aurbach, D. Promise and Reality of Post-Lithium-Ion Batteries with High Energy Densities. *Nat. Rev. Mater.* **2016**, *1*, 16013.
(4) Li, N. W.; Yin, Y. X.; Yang, C. P.; Guo, Y. G. An Artificial Solid Electrolyte Interphase Layer for Stable Lithium Metal Anodes. *Adv. Mater.* **2016**, *28*, 1853−1858.
(5) Harry, K. J.; Hallinan, D. T.; Parkinson, D. Y.; MacDowell, A. A.; Balsara, N. P. Detection of Subsurface Structures Underneath Dendrites Formed on Cycled Lithium Metal Electrodes. *Nat. Mater.* **2014**, *13*, 69−73.
(6) Xu, K. Nonaqueous Liquid Electrolytes for Lithium-Based Rechargeable Batteries. *Chem. Rev.* **2004**, *104*, 4303−4418.
(7) Wood, K. N.; Noked, M.; Dasgupta, N. P. Lithium Metal Anodes: Toward an Improved Understanding of Coupled Morphological, Electrochemical, and Mechanical Behavior. *ACS Energy Lett.* **2017**, *2*, 664−672.
(8) Quartarone, E.; Mustarelli, P. Electrolytes for Solid-State Lithium Rechargeable Batteries: Recent Advances and Perspectives. *Chem. Soc. Rev.* **2011**, *40*, 2525−2540.
(9) Lin, D.; Liu, Y.; Cui, Y. Reviving the Lithium Metal Anode for High-Energy Batteries. *Nat. Nanotechnol.* **2017**, *12*, 194−206.
(10) Tikekar, M. D.; Choudhury, S.; Tu, Z.; Archer, L. A. Design Principles for Electrolytes and Interfaces for Stable Lithium-Metal Batteries. *Nat. Energy* **2016**, *1*, 16114.
(11) Han, X.; Gong, Y.; Fu, K. K.; He, X.; Hitz, G. T.; Dai, J.; Pearse, A.; Liu, B.; Wang, H.; Rubloff, G.; Mo, Y.; Thangadurai, V.; Wachsman, E. D.; Hu, L. Negating Interfacial Impedance in Garnet-Based Solid-State Li Metal Batteries. *Nat. Mater.* **2017**, *16*, 572−579.
(12) Guo, X. Property Degradation of Tetragonal Zirconia Induced by Low-Temperature Defect Reaction with Water Molecules. *Chem. Mater.* **2004**, *16*, 3988−3994.

DOI: 10.1021/acsmaterialslett.9b00189
ACS Materials Lett. 2019, 1, 354−361

(13) Thangadurai, V.; Narayanan, S.; Pinzaru, D. Garnet-Type Solid-State Fast Li Ion Conductors for Li Batteries: Critical Review. *Chem. Soc. Rev.* **2014**, *43*, 4714−4727.
(14) Thangadurai, V.; Kaack, H.; Weppner, W. J. F. Novel Fast Lithium Ion Conduction in Garnet-Type $Li_5La_3M_2O_{12}$ (M = Nb, Ta). *J. Am. Ceram. Soc.* **2003**, *86*, 437−440.
(15) Wang, Y.; Richards, W. D.; Ong, S. P.; Miara, L. J.; Kim, J. C.; Mo, Y.; Ceder, G. Design Principles for Solid-State Lithium Superionic Conductors. *Nat. Mater.* **2015**, *14*, 1026−1031.
(16) Liu, T.; Ren, Y.; Shen, Y.; Zhao, S.-X.; Lin, Y.; Nan, C.-W. Achieving High Capacity in Bulk-Type Solid-State Lithium Ion Battery Based on $Li_{6.75}La_3Zr_{1.75}Ta_{0.25}O_{12}$ Electrolyte: Interfacial Resistance. *J. Power Sources* **2016**, *324*, 349−357.
(17) Chu, I.-H.; Kompella, C. S.; Nguyen, H.; Zhu, Z.; Hy, S.; Deng, Z.; Meng, Y. S.; Ong, S. P. Room-Temperature All-Solid-State Rechargeable Sodium-Ion Batteries with a Cl-Doped Na_3PS_4 Superionic Conductor. *Sci. Rep.* **2016**, *6*, 33733.
(18) Trevey, J.; Jang, J. S.; Jung, Y. S.; Stoldt, C. R.; Lee, S.-H. Glass−Ceramic $Li_2S-P_2S_5$ Electrolytes Prepared by a Single Step Ball Billing Process and Their Application for All-Solid-State Lithium−Ion Batteries. *Electrochem. Commun.* **2009**, *11*, 1830−1833.
(19) Nam, Y. J.; Cho, S.-J.; Oh, D. Y.; Lim, J.-M.; Kim, S. Y.; Song, J. H.; Lee, Y.-G.; Lee, S.-Y.; Jung, Y. S. Bendable and Thin Sulfide Solid Electrolyte Film: A New Electrolyte Opportunity for Free-Standing and Stackable High-Energy All-Solid-State Lithium-Ion Batteries. *Nano Lett.* **2015**, *15*, 3317−3323.
(20) Croce, F.; Persi, L.; Scrosati, B.; Serraino-Fiory, F.; Plichta, E.; Hendrickson, M. Role of the Ceramic Fillers in Enhancing the Transport Properties of Composite Polymer Electrolytes. *Electrochim. Acta* **2001**, *46*, 2457−2461.
(21) Gadjourova, Z.; Andreev, Y. G.; Tunstall, D. P.; Bruce, P. G. Ionic Conductivity in Crystalline Polymer Electrolytes. *Nature* **2001**, *412*, 520−523.
(22) Aetukuri, N. B.; Kitajima, S.; Jung, E.; Thompson, L. E.; Virwani, K.; Reich, M. L.; Kunze, M.; Schneider, M.; Schmidbauer, W.; Wilcke, W. W.; Bethune, D. S.; Scott, J. C.; Miller, R. D.; Kim, H.-C. Flexible Ion-Conducting Composite Membranes for Lithium Batteries. *Adv. Energy Mater.* **2015**, *5*, 1500265.
(23) Croce, F.; Appetecchi, G.; Persi, L.; Scrosati, B. Nanocomposite Polymer Electrolytes for Lithium Batteries. *Nature* **1998**, *394*, 456−458.
(24) Manthiram, A.; Yu, X.; Wang, S. Lithium Battery Chemistries Enabled by Solid-State Electrolytes. *Nat. Rev. Mater.* **2017**, *2*, 16103.
(25) Thangadurai, V.; Pinzaru, D.; Narayanan, S.; Baral, A. K. Fast Solid-State Li Ion Conducting Garnet-Type Structure Metal Oxides for Energy Storage. *J. Phys. Chem. Lett.* **2015**, *6*, 292−299.
(26) Ohta, S.; Kobayashi, T.; Asaoka, T. High Lithium Ionic Conductivity in the Garnet-Type Oxide $Li_{7-X}La_3(Zr_{2-X}, Nb_X)O_{12}$ (X = 0−2). *J. Power Sources* **2011**, *196*, 3342−3345.
(27) Kotobuki, M.; Munakata, H.; Kanamura, K.; Sato, Y.; Yoshida, T. Compatibility of $Li_7La_3Zr_2O_{12}$ Solid Electrolyte to All-Solid-State Battery Using Li Metal Anode. *J. Electrochem. Soc.* **2010**, *157*, A1076−A1079.
(28) Jin, Y.; Liu, K.; Lang, J.; Zhuo, D.; Huang, Z.; Wang, C.-a.; Wu, H.; Cui, Y. An Intermediate Temperature Garnet-Type Solid Electrolyte-Based Molten Lithium Battery for Grid Energy Storage. *Nature Energy* **2018**, *3*, 732.
(29) Pitawala, H.; Dissanayake, M.; Seneviratne, V. Combined Effect of Al_2O_3 Nano-Fillers and Ec Plasticizer on Ionic Conductivity Enhancement in the Solid Polymer Electrolyte $(PEO)_9$ LiTF. *Solid State Ionics* **2007**, *178*, 885−888.
(30) Scrosati, B.; Croce, F.; Persi, L. Impedance Spectroscopy Study of PEO-Based Nanocomposite Polymer Electrolytes. *J. Electrochem. Soc.* **2000**, *147*, 1718−1721.
(31) Li, Y.; Xu, B.; Xu, H.; Duan, H.; Lü, X.; Xin, S.; Zhou, W.; Xue, L.; Fu, G.; Manthiram, A.; Goodenough, J. B. Hybrid Polymer/Garnet Electrolyte with a Small Interfacial Resistance for Lithium-Ion Batteries. *Angew. Chem.* **2017**, *129*, 771−774.
(32) Van Den Broek, J.; Afyon, S.; Rupp, J. L. Interface-Engineered All-Solid-State Li-Ion Batteries Based on Garnet-Type Fast Li+ Conductors. *Adv. Energy Mater.* **2016**, *6*, 1600736.
(33) Gordon, Z. D.; Yang, T.; Gomes Morgado, G. B.; Chan, C. K. Preparation of Nano- and Microstructured Garnet $Li_7La_3Zr_2O_{12}$ Solid Electrolytes for Li-Ion Batteries Via Cellulose Templating. *ACS Sustainable Chem. Eng.* **2016**, *4*, 6391−6398.
(34) Sun, H. Y.; Sohn, H. J.; Yamamoto, O.; Takeda, Y.; Imanishi, N. Enhanced Lithium-Ion Transport in PEO-Based Composite Polymer Electrolytes with Ferroelectric $BaTiO_3$. *J. Electrochem. Soc.* **1999**, *146*, 1672−1676.
(35) Agrawal, R.; Pandey, G. Solid Polymer Electrolytes: Materials Designing and All-Solid-State Battery Applications: An Overview. *J. Phys. D: Appl. Phys.* **2008**, *41*, 223001.
(36) Liu, W.; Liu, N.; Sun, J.; Hsu, P.-C.; Li, Y.; Lee, H.-W.; Cui, Y. Ionic Conductivity Enhancement of Polymer Electrolytes with Ceramic Nanowire Fillers. *Nano Lett.* **2015**, *15*, 2740−2745.
(37) Fu, K. K.; Gong, Y.; Dai, J.; Gong, A.; Han, X.; Yao, Y.; Wang, C.; Wang, Y.; Chen, Y.; Yan, C.; Li, Y.; Wachsman, E. D.; Hu, L. Flexible, Solid-State, Ion-Conducting Membrane with 3d Garnet Nanofiber Networks for Lithium Batteries. *Proc. Natl. Acad. Sci. U. S. A.* **2016**, *113*, 7094−7099.
(38) Yang, T.; Zheng, J.; Cheng, Q.; Hu, Y.-Y.; Chan, C. K. Composite Polymer Electrolytes with $Li_7La_3Zr_2O_{12}$ Garnet-Type Nanowires as Ceramic Fillers: Mechanism of Conductivity Enhancement and Role of Doping and Morphology. *ACS Appl. Mater. Interfaces* **2017**, *9*, 21773−21780.
(39) Thorat, I. V.; Stephenson, D. E.; Zacharias, N. A.; Zaghib, K.; Harb, J. N.; Wheeler, D. R. Quantifying Tortuosity in Porous Li-Ion Battery Materials. *J. Power Sources* **2009**, *188*, 592−600.
(40) Sander, J.; Erb, R.; Li, L.; Gurijala, A.; Chiang, Y.-M. High-Performance Battery Electrodes Via Magnetic Templating. *Nat. Energy* **2016**, *1*, 16099.
(41) Billaud, J.; Bouville, F.; Magrini, T.; Villevieille, C.; Studart, A. R. Magnetically Aligned Graphite Electrodes for High-Rate Performance Li-Ion Batteries. *Nat. Energy* **2016**, *1*, 16097.
(42) Zhai, H.; Xu, P.; Ning, M.; Cheng, Q.; Mandal, J.; Yang, Y. A Flexible Solid Composite Electrolyte with Vertically Aligned and Connected Ion-Conducting Nanoparticles for Lithium Batteries. *Nano Lett.* **2017**, *17*, 3182−3187.
(43) Wang, X.; Zhai, H.; Qie, B.; Cheng, Q.; Li, A.; Borovilas, J.; Xu, B.; Shi, C.; Jin, T.; Liao, X.; Li, Y.; He, X.; Du, S.; Fu, Y.; Dontigny, M.; Zaghib, K.; Yang, Y. Rechargeable Solid-State Lithium Metal Batteries with Vertically Aligned Ceramic Nanoparticle/Polymer Composite Electrolyte. *Nano Energy* **2019**, *60*, 205−212.
(44) Wan, J.; Xie, J.; Kong, X.; Liu, Z.; Liu, K.; Shi, F.; Pei, A.; Chen, H.; Chen, W.; Chen, J.; Zhang, X.; Zong, L.; Wang, J.; Chen, L.-Q.; Qin, J.; Cui, Y. Ultrathin, Flexible, Solid Polymer Composite Electrolyte Enabled with Aligned Nanoporous Host for Lithium Batteries. *Nat. Nanotechnol.* **2019**, *14*, 705−711.
(45) Liu, W.; Lee, S. W.; Lin, D.; Shi, F.; Wang, S.; Sendek, A. D.; Cui, Y. Enhancing Ionic Conductivity in Composite Polymer Electrolytes with Well-Aligned Ceramic Nanowires. *Nat. Energy* **2017**, *2*, 17035.
(46) Wu, J.-F.; Chen, E.-Y.; Yu, Y.; Liu, L.; Wu, Y.; Pang, W.-K.; Peterson, V. K.; Guo, X. Gallium-Doped $Li_7La_3Zr_2O_{12}$ Garnet-Type Electrolytes with High Lithium-Ion Conductivity. *ACS Appl. Mater. Interfaces* **2017**, *9*, 1542−1552.
(47) Buschmann, H.; Dolle, J.; Berendts, S.; Kuhn, A.; Bottke, P.; Wilkening, M.; Heitjans, P.; Senyshyn, A.; Ehrenberg, H.; Lotnyk, A.; Duppel, V.; Kienle, L.; Janek, J. Structure and Dynamics of the Fast Lithium Ion Conductor "$Li_7La_3Zr_2O_{12}$". *Phys. Chem. Chem. Phys.* **2011**, *13*, 19378−19392.
(48) Christie, A. M.; Lilley, S. J.; Staunton, E.; Andreev, Y. G.; Bruce, P. G. Increasing the Conductivity of Crystalline Polymer Electrolytes. *Nature* **2005**, *433*, 50−53.
(49) Cheng, S.; Smith, D. M.; Pan, Q.; Wang, S.; Li, C. Y. Anisotropic Ion Transport in Nanostructured Solid Polymer Electrolytes. *RSC Adv.* **2015**, *5*, 48793−48810.

DOI: 10.1021/acsmaterialslett.9b00189
ACS Materials Lett. 2019, 1, 354−361

(50) Liu, W.; Lin, D.; Sun, J.; Zhou, G.; Cui, Y. Improved Lithium Ionic Conductivity in Composite Polymer Electrolytes with Oxide-Ion Conducting Nanowires. *ACS Nano* **2016**, *10*, 11407−11413.
(51) Zheng, J.; Hu, Y. Y. New Insights into Compositional Dependence of Li-Ion Transport in Polymer-Ceramic Composite Electrolytes. *ACS Appl. Mater. Interfaces* **2018**, *10*, 4113−4120.
(52) Zheng, J.; Tang, M.; Hu, Y. Y. Lithium Ion Pathway within $Li_7La_3Zr_2O_{12}$-Polyethylene Oxide Composite Electrolytes. *Angew. Chem.* **2016**, *128*, 12726−12730.
(53) Jayathilaka, P.; Dissanayake, M.; Albinsson, I.; Mellander, B.-E. Effect of Nano-Porous Al_2O_3 on Thermal, Dielectric and Transport Properties of the (PEO)9LiTFSi Polymer Electrolyte System. *Electrochim. Acta* **2002**, *47*, 3257−3268.
(54) Croce, F.; Focarete, M. L.; Hassoun, J.; Meschini, I.; Scrosati, B. A Safe, High-Rate and High-Energy Polymer Lithium-Ion Battery Based on Gelled Membranes Prepared by Electrospinning. *Energy Environ. Sci.* **2011**, *4*, 921−927.

DOI: 10.1021/acsmaterialslett.9b00189
ACS Materials Lett. 2019, 1, 354−361